

# Baryon Number and Electric Charge Fluctuations in High Energy Nucleus-Nucleus Collisions

V.P. Konchakovski,<sup>1,2,3</sup> M.I. Gorenstein,<sup>1,3</sup> E.L. Bratkovskaya,<sup>3</sup> and H. Stöcker<sup>3,4</sup>

<sup>1</sup>*Bogolyubov Institute for Theoretical Physics, Kiev, Ukraine*

<sup>2</sup>*Shevchenko National University, Kiev, Ukraine*

<sup>3</sup>*Frankfurt Institute for Advanced Studies, Frankfurt, Germany*

<sup>4</sup>*Institut für Theoretische Physik, Johann Wolfgang Goethe Universität, Frankfurt, Germany*

## Abstract

Event-by-event fluctuations of the net baryon number and electric charge in nucleus-nucleus collisions are studied in Pb+Pb at 158 AGeV within the HSD transport model. We reveal an important role of the fluctuations in the number of target nucleon participants. They strongly influence all measured fluctuations even in the samples of events with rather rigid centrality trigger. This fact can be used to check different scenarios of nucleus-nucleus collisions by measuring the multiplicity fluctuations as a function of collision centrality in fixed kinematical regions of the projectile and target hemispheres.

PACS numbers:

Keywords:

## I. INTRODUCTION

The aim of the present paper is to study the fluctuations of the net baryon number and electric charge in high energy nucleus-nucleus (A+A) collisions. We use the HSD [1] transport approach which reproduces both the different particle multiplicities and longitudinal differential rapidity distributions for central collisions of Au+Au (or Pb+Pb) from AGS to SPS energies rather well [2]. The fluctuations in high energy nuclear collisions (see, e.g., Refs. [3, 4, 5, 6, 7, 8, 9, 10, 11, 12] and references therein) reveal a new physical information. The fluctuations in A+A collisions are studied on an event-by-event basis: a given observable is measured in each event and the fluctuations are evaluated for a specially selected set of these events. The statistical model has been successfully used to describe the data on hadron multiplicities in relativistic A+A collisions (see, e.g., Ref. [13] and a recent review [14]) as well as in elementary particle collisions [15]. This gives rise to the question whether the fluctuations, in particular the multiplicity fluctuations, do also follow the statistical hadron-resonance gas results. Recently the particle number fluctuations have been studied in different statistical ensembles [16]. The statistical fluctuations can be closely related to phase transitions in QCD matter, with specific signatures for 1-st and 2-nd order phase transitions as well as for the critical point [6, 7].

In addition to the statistical fluctuations, the complicated dynamics of A+A collisions generates *dynamical* fluctuations. The fluctuations in the initial energy deposited inelastically in the statistical system yield *dynamical* fluctuations of all macroscopic parameters, like the total entropy or strangeness content. The observable consequences of the initial energy density fluctuations are sensitive to the equation of state of the matter, and can therefore be useful as signals for phase transitions [12]. Even when the data are obtained with a centrality trigger, the number of nucleons participating in inelastic collisions still fluctuates considerably. In the language of statistical mechanics, these fluctuations in participant nucleon number correspond to volume fluctuations. Secondary particle multiplicities scale linearly with the volume, hence, volume fluctuations translate directly to particle number fluctuations.

The present work is a continuation of our recent study [17] where we have analyzed the charged particle number fluctuations in Pb+Pb collisions at 158 AGeV within the UrQMD and HSD transport approaches. The net baryon number and electric charge event-by-event

fluctuations are studied in different rapidity regions of the projectile and target hemispheres.

The paper is organized as follows. Section II presents the HSD results for the fluctuations of the number of nucleon participants while Sections III and IV give the net baryon number fluctuations and electric charge fluctuations, respectively. In Section V we discuss the fluctuations in the samples of most central collisions whereas Section VI finally concludes the present study.

## II. FLUCTUATIONS OF THE NUMBER OF PARTICIPANTS

In each A+A collision only a fraction of all  $2A$  nucleons interact. These are called participant nucleons and are denoted as  $N_P^{proj}$  and  $N_P^{targ}$  for the projectile and target nuclei, respectively. The nucleons, which do not interact, are called the projectile and target spectators,  $N_S^{proj} = A - N_P^{proj}$  and  $N_S^{targ} = A - N_P^{targ}$ . The fluctuations in high energy A+A collisions are dominated by a geometrical variation of the impact parameter. However, even for the fixed impact parameter the number of participants,  $N_P \equiv N_P^{proj} + N_P^{targ}$ , fluctuates from event to event. This is due to the fluctuations of the initial states of the colliding nuclei and the probabilistic character of the interaction process. The fluctuations of  $N_P$  form usually a large and uninteresting background. In order to minimize its contribution the NA49 Collaboration has selected samples of collisions with a fixed numbers of projectile participants. This selection is possible due to a measurement of  $N_S^{proj}$  in each individual collision by a calorimeter which covers the projectile fragmentation domain. However, even in the samples with  $N_P^{proj} = const$  the number of target participants fluctuates considerably. Hence, an asymmetry between projectile and target participants is introduced, i.e.  $N_P^{proj}$  is constant by constraint, whereas  $N_P^{targ}$  fluctuates independently.

In the following the variance,  $Var(n) \equiv \langle n^2 \rangle - \langle n \rangle^2$ , and scaled variance,  $\omega_n \equiv Var(n)/\langle n \rangle$ , where  $n$  stands for a given random variable and  $\langle \dots \rangle$  for event-by-event averaging, will be used to quantify fluctuations. In each sample with  $N_P^{proj} = const$  the number of target participants fluctuates around its mean value,  $\langle N_P^{targ} \rangle$ , with the scaled variance  $\omega_P^{targ}$ . From an output of the HSD minimum bias simulations of Pb+Pb collisions at 158 AGeV we form the samples of events with fixed values of  $N_P^{proj}$ . Fig. 1 presents the HSD average value  $\langle N_P^{targ} \rangle$  (left) and the scaled variances  $\omega_P^{targ}$  (right) as functions of  $N_P^{proj}$ . One finds  $\langle N_P^{targ} \rangle \simeq N_P^{proj}$ ; the deviations are only seen at very small ( $N_P^{proj} \approx 1$ ) and very large

( $N_P^{proj} \approx A$ ) numbers of projectile participants. The fluctuations of  $N_P^{targ}$  are quite strong:  $\omega_P^{targ} > 2$  at  $N_P^{proj} = 10 - 80$ .

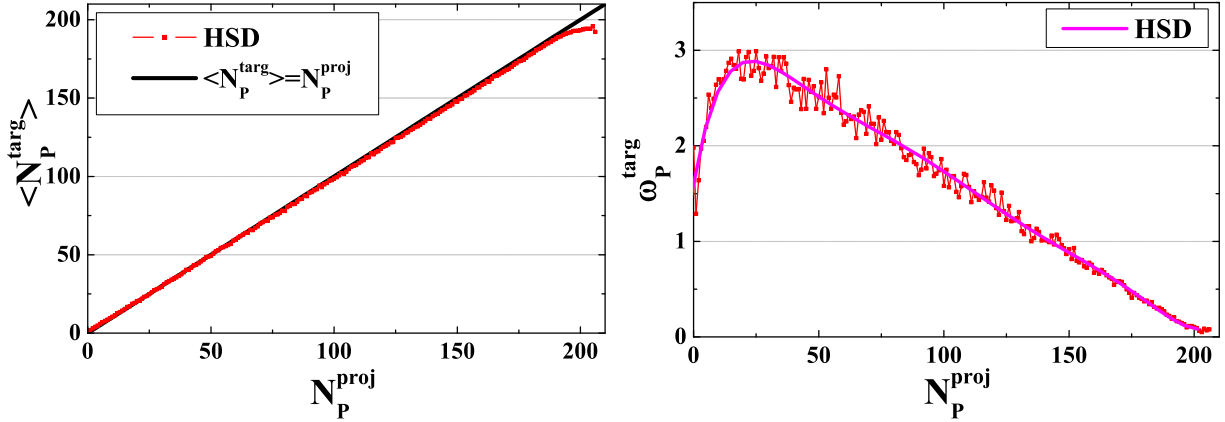


FIG. 1: The HSD simulations in Pb+Pb collisions at 158 AGeV for the average value  $\langle N_P^{targ} \rangle$  (left) and the scaled variances  $\omega_P^{targ}$  (right) as functions of  $N_P^{proj}$ .

The consequences of the asymmetry between projectile and target hemispheres depend on the A+A dynamics. Following Ref. [18] different models of hadron production in relativistic A+A collisions can be divided into three limiting groups: transparency, mixing, and reflection models. The first group assumes that the final longitudinal flows of the hadron production sources – related to projectile and target participants – follow in the directions of the projectile and target, respectively. We call this group of models transparency (T-)models. If the projectile and target flows of hadron production sources are mixed, we call these models the mixing (M-)models. Finally, one may even speculate that the initial flows are reflected in the collision process. The projectile related matter then flows in the direction of the target and the target related matter flows in the direction of the projectile. This class of models we call the reflection (R-)models. The rapidity distributions resulting from the T-, M-, and R-models are sketched in Fig. 2 taken from Ref. [18].

One expects large fluctuations of hadron multiplicities in the domain of the target related flow and small fluctuations in the domain of the projectile related flow. When both flows are mixed, intermediate fluctuations are predicted. The multiplicity fluctuations in the projectile momentum hemisphere are larger than those in the target hemisphere in T-models. The opposite relation is predicted for R-models, whereas for M-models the fluctuations in the projectile and target hemispheres are expected to be the same.

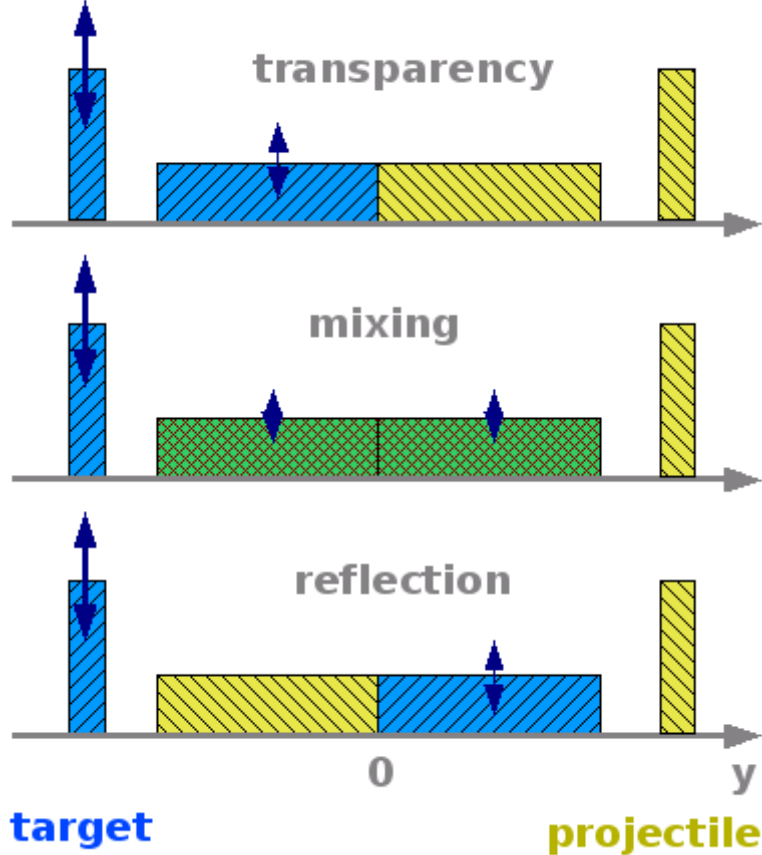


FIG. 2: The sketch of the rapidity distributions of the baryon number or the particle production sources (horizontal rectangles) in nucleus-nucleus collisions resulting from the transparency, mixing and reflection models. The spectator nucleons are indicated by the vertical rectangles. In the collisions with a fixed number of projectile spectators only matter related to the target shows significant fluctuations (vertical arrows).

### III. NET BARYON NUMBER FLUCTUATIONS

Let us begin a quantitative discussion by first considering the fluctuations of the net baryon number in different regions of the participant domain in collisions of two identical nuclei. These fluctuations are most closely related to the fluctuations of the number of participant nucleons because of baryon number conservation. The HSD results for  $\omega_B$  in Pb+Pb at 158 AGeV are presented in Fig. 3.

In each event we subtract the nucleon spectators when counting the number of baryons. The net baryon number in the full phase space,  $B \equiv N_B - N_{\bar{B}}$ , equals then to the total number of participants  $N_P = N_P^{targ} + N_P^{proj}$ . At fixed  $N_P^{proj}$  the  $N_P$  number fluctuates due to

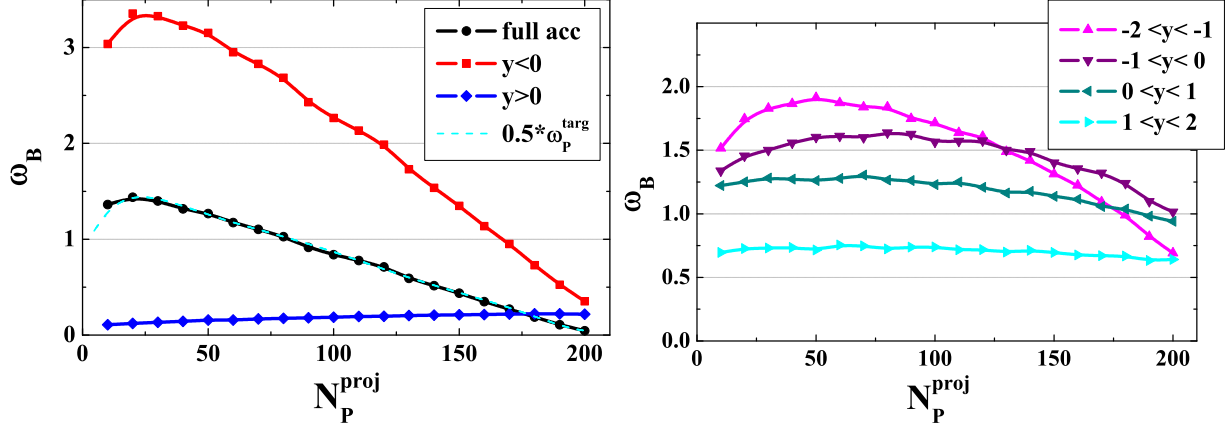


FIG. 3: The HSD simulations for Pb+Pb collisions at 158 AGeV for fixed values of  $N_P^{proj}$ . *Left:* The baryon number fluctuations in full acceptance,  $\omega_B$ , in projectile hemisphere,  $\omega_B^p$  (lower curve), and in target hemisphere,  $\omega_B^t$  (upper curve). The dashed line,  $0.5 \omega_P^{targ}$ , demonstrates the validity of the relation (1). *Right:* The scaled variances of the baryon number fluctuations in different rapidity intervals.

fluctuations of  $N_P^{targ}$ . These fluctuations correspond to an average value,  $\langle N_P^{targ} \rangle \simeq N_P^{proj}$ , and a scaled variance,  $\omega_P^{targ}$  (see Fig. 1). Thus, for the net baryon number fluctuations in the full phase space we find,

$$\omega_B = \frac{Var(N_P)}{\langle N_P \rangle} \simeq \frac{\langle (N_P^{targ})^2 \rangle - \langle N_P^{targ} \rangle^2}{2\langle N_P^{targ} \rangle} = \frac{1}{2} \omega_P^{targ}. \quad (1)$$

A factor 1/2 in the right hand side of Eq. (1) appears because only half of the total number of participants fluctuates.

Let us introduce  $\omega_B^p$  and  $\omega_B^t$ , where the superscripts  $p$  and  $t$  mark quantities measured in the projectile and target momentum hemispheres, respectively. Fig. 3 demonstrates that  $\omega_B^p > \omega_B^t$ , both in the whole projectile-target hemispheres and in the symmetric rapidity intervals. On the other hand one observes that  $\omega_B^p \approx \omega_B^t$  in most central collisions. This is because the fluctuations of the target participants become negligible in this case, i.e.  $\omega_P^{targ} \rightarrow 0$  (Fig.1, right). As a consequence the fluctuations of any observable in the symmetric rapidity intervals become identical in most central collisions.

By assumption, the mixing of the projectile and target participants is absent in T- and R-models. Therefore, in T-models, the net baryon number in the projectile hemisphere equals to  $N_p^{proj}$  and does not fluctuate, i.e.  $\omega_B^p(T) = 0$ , whereas the net baryon number in

the target hemisphere equals to  $N_p^{targ}$  and fluctuates with  $\omega_B^t(T) = \omega_P^{targ}$ . These relations are reversed in R-models. We introduce now a mixing of baryons between the projectile and target hemispheres. Let  $\alpha$  be the probability for (projectile) target participant to be detected in the (target) projectile hemisphere. We denote by  $n^t$  and  $n^p$  the number of baryons which end up in the target and projectile hemisphere, respectively, from the opposite hemisphere. Then the probabilities to detect  $B^t$  baryons in the target hemisphere, and  $B^p$  baryons in the projectile hemisphere, can be written as,

$$P(B^t; N_P^{proj}) = \sum_{N_P^{targ}} W(N_P^{targ}; N_P^{proj}) \sum_{n^t=1}^{N_P^{targ}} \sum_{n^p=1}^{N_P^{proj}} \alpha^{n^p} (1-\alpha)^{N_P^{targ}-n^p} \frac{N_P^{targ}!}{n^p!(N_P^{targ}-n^p)!} \\ \times \alpha^{n^t} (1-\alpha)^{N_P^{proj}-n^t} \frac{N_P^{proj}!}{n^t!(N_P^{proj}-n^t)!} \delta(B^t - N_P^{targ} - n^t + n^p), \quad (2)$$

$$P(B^p; N_P^{proj}) = \sum_{N_P^{targ}} W(N_P^{targ}; N_P^{proj}) \sum_{n^t=1}^{N_P^{targ}} \sum_{n^p=1}^{N_P^{proj}} \alpha^{n^p} (1-\alpha)^{N_P^{targ}-n^p} \frac{N_P^{targ}!}{n^p!(N_P^{targ}-n^p)!} \\ \times \alpha^{n^t} (1-\alpha)^{N_P^{proj}-n^t} \frac{N_P^{proj}!}{n^t!(N_P^{proj}-n^t)!} \delta(B^p - N_P^{proj} - n^p + n^t), \quad (3)$$

where  $W(N_P^{targ}; N_P^{proj})$  is the probability distribution of  $N_P^{targ}$  in a sample with fixed value of  $N_P^{proj}$ . From Eqs. (2,3) with a straightforward calculation we find:

$$\omega_B^t = (1-\alpha)^2 \omega_P^{targ} + 2\alpha(1-\alpha), \quad \omega_B^p = \alpha^2 \omega_P^{targ} + 2\alpha(1-\alpha). \quad (4)$$

A (complete) mixing of the projectile and target participants is assumed in M-models. Thus each participant nucleon with equal probability,  $\alpha = 1/2$ , can be found either in the target or in projectile hemispheres. In M-models the fluctuations in both projectile and target hemispheres are identical. The limiting cases,  $\alpha = 0$  and  $\alpha = 1$ , of Eq. (4) correspond to T- and R-models, respectively. In summary the scaled variances of the net baryon number fluctuations in the projectile,  $\omega_B^p$ , and target,  $\omega_B^t$ , hemispheres are:

$$\omega_B^p(T) = 0, \quad \omega_B^t(T) = \omega_P^{targ}, \quad (5)$$

$$\omega_B^p(M) = \omega_B^t(M) = \frac{1}{2} + \frac{1}{4} \omega_P^{targ}, \quad (6)$$

$$\omega_B^p(R) = \omega_P^{targ}, \quad \omega_B^t(R) = 0, \quad (7)$$

in the T- (5), M- (6) and R- (7) models of the baryon number flow. The different models lead to significantly different predictions for  $\omega_B^p$  and  $\omega_B^t$ .

In Fig. 4 we show the predictions of T-, M- and R-models (5-7) with  $\omega_P^{targ}$  from Fig. 1 for Pb+Pb collisions at 158A GeV. From Fig. 4 one concludes that the HSD results are

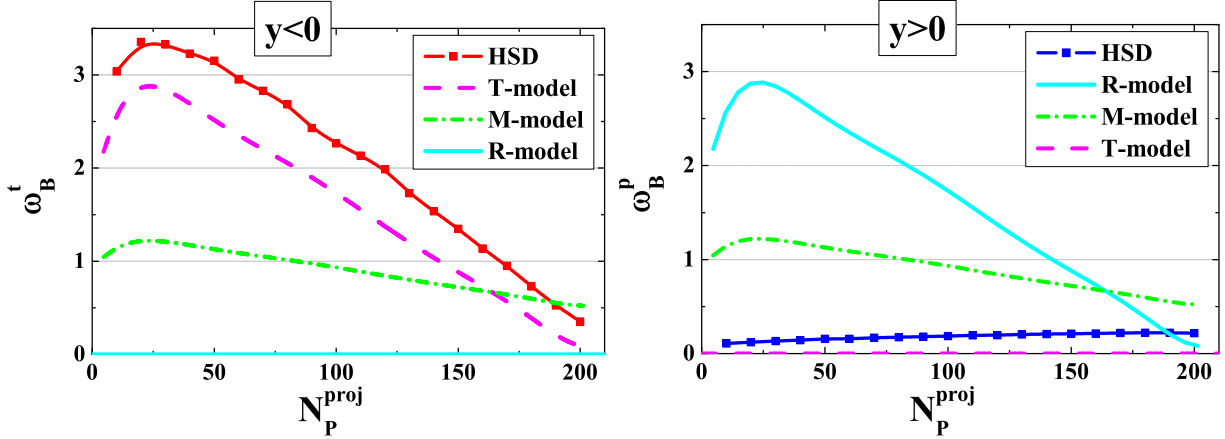


FIG. 4: The  $\omega_B^t$  (left) and  $\omega_B^p$  (right) of the HSD simulations in comparison to T-, M- and R-models (5-7), with  $\omega_P^{targ}$  taken from Fig. 1.

close to the T-model estimates for baryon flow. However, the deviation from the results (5) are clearly seen:  $\omega_B^p > 0$  and  $\omega_B^t > \omega_P^{targ}$ . One can not fit the HSD values of  $\omega_B^t$  and  $\omega_B^p$  by Eq. (4). To make  $\omega_B^p > 0$  one needs  $\alpha > 0$ , but this induces  $\omega_B^t < \omega_P^{targ}$ , i.e. a mixing of baryons between the projectile and target hemispheres creates a non-zero baryon number fluctuations in the projectile hemisphere on the expense of fluctuations in the target hemisphere. Indeed, it follows from Eq. (4) that  $\omega_B^p$  increases with  $\alpha$  for all  $\alpha$ , if  $\omega_P^{targ} > 1$ , and for  $\alpha < (2 - \omega_P^{targ})^{-1}$ , if  $\omega_P^{targ} < 1$ . On the other hand,  $\omega_B^t$  increases with  $\alpha$  if  $\alpha < (1 - \omega_P^{targ})(2 - \omega_P^{targ})^{-1}$ . This shows that an increase of  $\omega_B^t$  with  $\alpha$  is only possible for  $\omega_P^{targ} < 1$ . Thus for  $\omega_P^{targ} > 1$  one finds an increase of  $\omega_B^p$  with  $\alpha$  and a decrease of  $\omega_B^t$  with  $\alpha$  for all physical values of  $\alpha$  from 0 to 1. Therefore, we conclude that the HSD values of  $\omega_B^t$  (i.e. the fact that  $\omega_B^t > \omega_P^{targ}$ ) can not be explained by Eq. (4) with  $\alpha > 0$ .

The numbers of target and projectile participants are defined as  $N_P^{targ} \equiv A - N_S^{targ}$  and  $N_P^{proj} \equiv A - N_S^{proj}$ . The actual event-by-event numbers of baryons in the target and projectile hemispheres,  $N_B^t$  and  $N_B^p$ , may differ from  $N_P^{targ}$  and  $N_P^{proj}$ . This is because transfer of baryons between the projectile and target hemispheres arise from the production of baryon-antibaryon pairs. The partners of each newly created  $b\bar{b}$ -pair can be with non-zero probability detected in different hemispheres. We introduce  $b^t \equiv N_B^t - N_P^{targ}$  and number of antibaryons in the target hemisphere,  $\bar{b}^t$ . Similarly,  $b^p \equiv N_B^p - N_P^{proj}$ , and  $\bar{b}^p$  is the number

of antibaryons in the projectile hemisphere. One finds:

$$\omega_B^t \equiv \frac{Var(N_P^{targ} + b^t - \bar{b}^t)}{\langle B^t \rangle} = \omega_P^{targ} + \frac{1}{N_P^{proj}} \left[ Var(b^t) + Var(\bar{b}^t) + 2 \Delta(N_P^{targ}, b^t) - 2 \Delta(N_P^{targ}, \bar{b}^t) - 2 \Delta(b^t, \bar{b}^t) \right], \quad (8)$$

$$\omega_B^p \equiv \frac{Var(N_P^{proj} + b^p - \bar{b}^p)}{\langle B^p \rangle} = \frac{1}{N_P^{proj}} \left[ Var(b^p) + Var(\bar{b}^p) - 2 \Delta(b^p, \bar{b}^p) \right], \quad (9)$$

where

$$\Delta(N_1, N_2) \equiv \langle N_1 \cdot N_2 \rangle - \langle N_1 \rangle \cdot \langle N_2 \rangle. \quad (10)$$

As  $N_P^{proj} = const$  in the sample, it follows that  $\omega_P^{proj} = 0$ ,  $\Delta(N_P^{proj}, b^p) = 0$ ,  $\Delta(N_P^{proj}, \bar{b}^p) = 0$ , and these terms are absent in the r.h.s. of Eq. (9). Different terms of Eq. (8) and Eq. (9) found from the HSD simulations are presented in Fig 5. One observes that terms

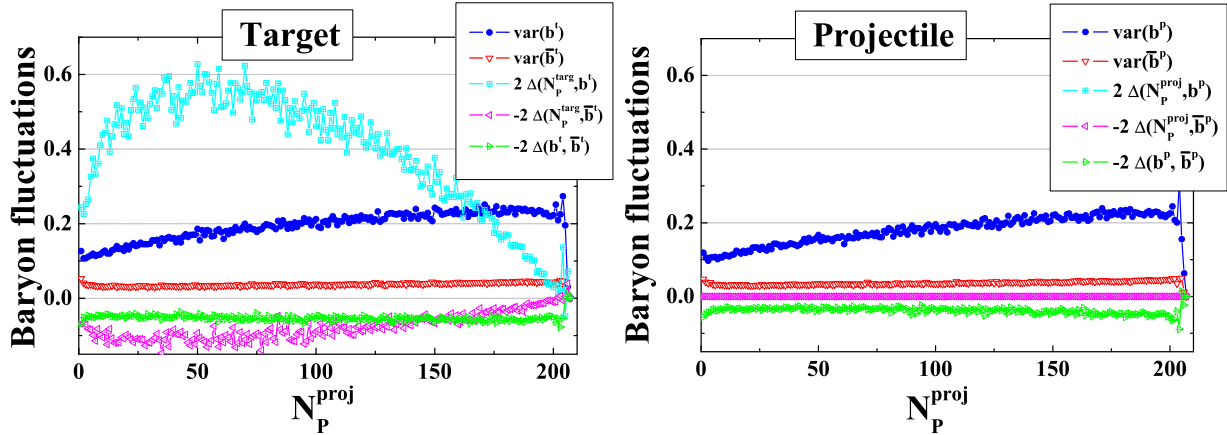


FIG. 5: Different terms of Eq. (8), *left*, and Eq. (9), *right*, are presented as a function of  $N_P^{proj}$ .

of Eq. (8,9) expressing the fluctuations of antibaryons,  $Var(\bar{b}^p)/N_P^{proj}$ , and the correlation terms,  $2\Delta(N_P^{targ}, \bar{b}^t)/N_P^{proj}$  and  $-2\Delta(b^t, \bar{b}^t)/N_P^{proj}$ , with antibaryons included, are small. Therefore, one finds,  $\omega_B^p \cong Var(b^p)/N_P^{proj}$ . In the target hemisphere, the  $\omega_P^{targ}$  gives the main contribution to  $\omega_B^t$  in Eq. (8). The term  $Var(b^t)/N_P^{proj}$  also contributes to  $\omega_B^t$ , similarly to that,  $Var(b^p)/N_P^{proj}$ , in the projectile hemisphere. However, the main additional term to  $\omega_B^t$  is  $2\Delta(N_P^{targ}, b^t)/N_P^{proj}$ , which is due to (positive) correlations between  $N_P^{targ}$  and  $b^t$ . This implies that in events with large  $N_P^{targ}$  (i.e.  $N_P^{targ} > \langle N_P^{targ} \rangle \cong N_P^{proj}$ ) some additional baryons move from the projectile to the target hemisphere, and when  $N_P^{targ}$  is small (i.e.

$N_P^{targ} < \langle N_P^{targ} \rangle \cong N_P^{proj}$ ) the baryons move in a reverse direction from the target to the projectile hemisphere. This is shown in Fig. 6.

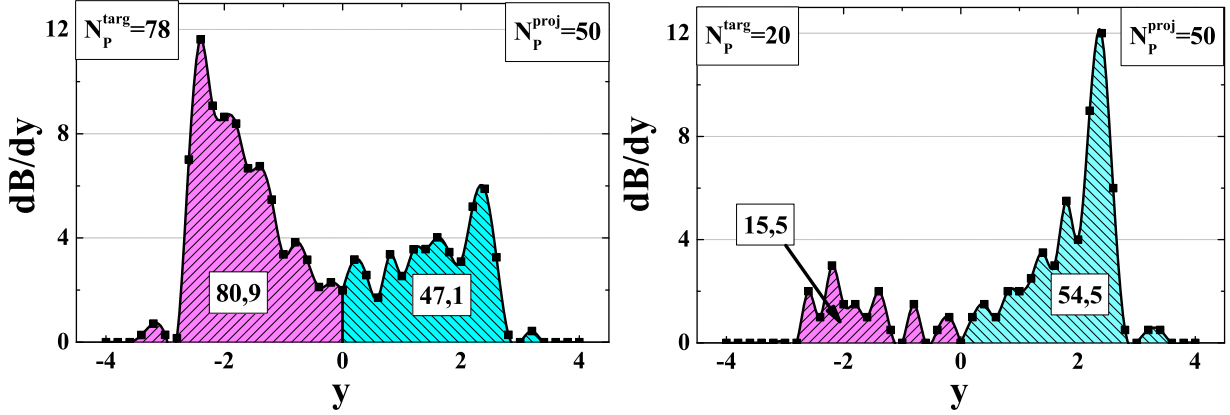


FIG. 6: The HSD results for Pb+Pb collisions at 158 AGeV for the rapidity distributions of baryon numbers in nonsymmetric samples with  $N_P^{proj} = 50, N_P^{targ} = 78$  (left), and  $N_P^{proj} = 50, N_P^{targ} = 20$  (right).

This HSD result looks rather unexpected. We remind that Eq. (4) predicts for  $\omega_B^t$  the opposite behavior: due to a simple mixing of baryons between the target and projectile hemispheres the initially large fluctuations,  $\omega_P^{targ}$ , are transformed into smaller ones,  $\omega_B^t$ . It seems that the origin of this effect is the following: For  $N_P^{targ} > N_P^{proj}$  each projectile nucleon interacts, in average, more often than the target nucleon. The projectile participant loses then a larger part of its energy, and in the rapidity space its position becomes closer to  $y_{c.m.} = 0$  than the position of target participants. This gives to projectile participants more chances to move due to further rescatterings from projectile to target hemisphere, in a comparison with target participants to move in the opposite direction. For  $N_P^{targ} < N_P^{proj}$  there is a reverse situation. This fact was not taken into account in Eqs. (2,3) where it has been assumed that the mixing probability  $\alpha$  is the same for projectile and target participants, and independent of  $N_P^{targ}$ .

#### IV. NET ELECTRIC CHARGE FLUCTUATIONS

The T-, M- and R-models give very different predictions for  $\omega_B^p$  and  $\omega_B^t$  for the samples of events with fixed values of  $N_P^{targ}$ . Additional interesting correlations between the  $B^t$  and  $B^p$  numbers, as those seen in the HSD simulations, can be expected. Unfortunately, they

may be difficult to test experimentally as an identification of protons and a measurement of neutrons in a large acceptance in a single event is difficult. Measurements of the charged particle multiplicity in a large acceptance can be performed with the existing detectors. In this section we consider the HSD results for the net electric charge,  $Q$ , fluctuations. As  $Q \cong 0.4B$  in the initial heavy nuclei one can naively expect that  $Q$  fluctuations are quite similar to  $B$  fluctuations. We stress, however, a principal difference between  $Q$  and  $B$  in relativistic A+A collisions. Fig. 7 demonstrates the rapidity distributions of the net baryon number,  $B = N_B - N_{\bar{B}}$  (left), and *total* number of baryons,  $N_B + N_{\bar{B}}$  (right), for different centralities in Pb+Pb collisions at 158 AGeV. One observes that both quantities are very close to each other; the  $y$ -dependence and absolute values are very close for  $B$  and  $N_B - N_{\bar{B}}$  distributions. This is, of course, because the number of baryons is rather small,  $N_{\bar{B}} \ll N_B$ .

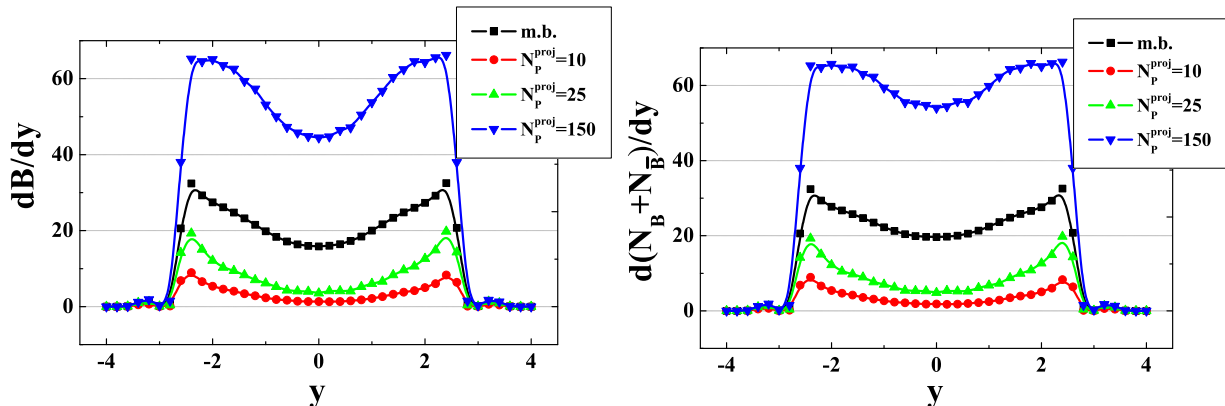


FIG. 7: The HSD rapidity distributions in Pb+Pb collisions at 158 AGeV for the net baryon number,  $B = N_B - N_{\bar{B}}$  (left), and total number of baryons,  $N_B + N_{\bar{B}}$  (right), at different  $N_P^{proj}$  and in the minimum bias (m.b.) sample.

Fig. 8 shows the same as Fig. 7 but for the electric charge  $Q = N_+ - N_-$  (left), and *total* number of charged particles,  $N_{ch} \equiv N_+ + N_-$  (right). The  $y$ -dependence of  $dQ/dy$  and  $dN_{ch}/dy$  is quite different. Besides, the absolute values of  $N_{ch}$  are about 10 times larger than those of  $Q$ . This implies that  $Q \ll N_+ \approx N_-$ .

In the previous section we have used the scaled variance  $\omega_B$  to quantify the measure of the net baryon fluctuations. It appears to be a useful variable as  $\omega_B$  is straightforwardly connected to  $\omega_P^{targ}$  and due to the relatively small number of antibaryons. Fig. 8 tells that  $\omega_Q$  is a bad measure of the electric charge fluctuations in high energy A+A collisions. One observes that  $\omega_Q \equiv Var(Q)/\langle Q \rangle$  is much larger than 1 simply due to the small value of  $\langle Q \rangle$

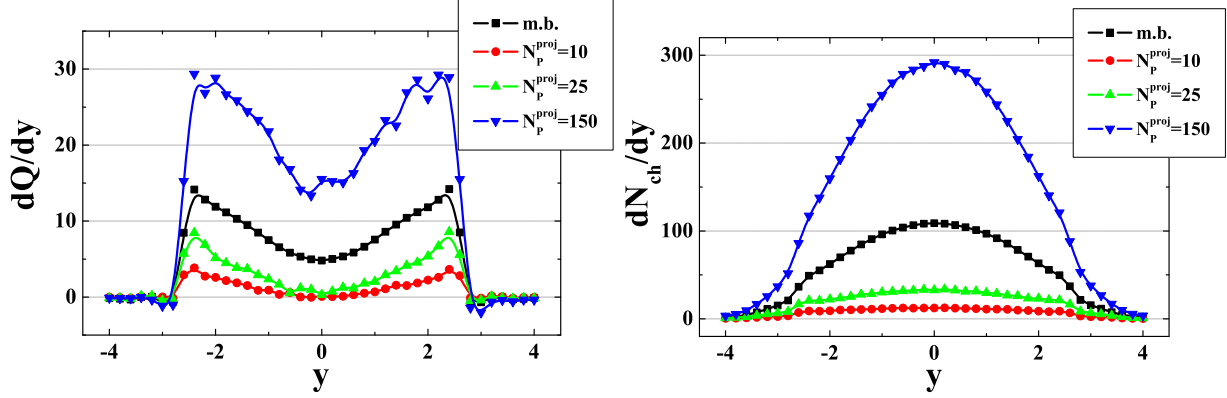


FIG. 8: The same as in Fig. 7 but for the electric charge  $Q = N_+ - N_-$  (left), and total number of charged particles,  $N_{ch} \equiv N_+ + N_-$  (right).

in a comparison with  $N_+$  and  $N_-$ . If the A+A collision energy increases, it follows,  $\langle Q \rangle \rightarrow 0$ , and thus  $\omega_Q \rightarrow \infty$ . The same will happen with  $\omega_B$  too at much larger than the SPS energy. A useful measure of the net electric charge fluctuations is the quantity (see, e.g., [10]):

$$X_Q \equiv \frac{Var(Q)}{\langle N_{ch} \rangle}. \quad (11)$$

A value of  $X_Q$  can be easily calculated for the Boltzmann ideal gas in the grand canonical ensemble. In this case the number of negative and positive particles fluctuates according to the Poisson distribution (i.e.  $\omega_- = \omega_+ = 1$ ), and the correlation between  $N_+$  and  $N_-$  are absent (i.e.  $\langle N_+ N_- \rangle = \langle N_+ \rangle \langle N_- \rangle$ ), so that  $X_Q = 1$ . On the other hand, the canonical ensemble formulation (i.e. when  $Q = const$  fixed exactly for all microscopic states of the system) leads to  $X_Q = 0$ . Fig. 9 shows the results of the HSD simulations for the full acceptance, for the projectile and target hemispheres (left), and also for symmetric rapidity intervals in the c.m.s. (right).

The  $Q$  fluctuation in the full acceptance is due to  $N_P^{targ}$  fluctuations. As  $Q \cong 0.4B$  in colliding (heavy) nuclei, one may expect  $Var(Q) \cong 0.16 Var(B)$ . In addition,  $\langle N_{ch} \rangle \cong 4\langle N_P \rangle$  at 158 AGeV, so that one estimates  $X_Q \cong 0.04 \omega_B$  for the fluctuations in the full phase space. The actual values of  $X_Q$  presented in Fig. 9 (left) are about 3 times larger. This is because of  $Q$  fluctuations due to different event-by-event values of proton and neutron participants even in a sample with fixed values of  $N_P^{proj}$  and  $N_P^{targ}$ .

From Fig. 9 (right) one sees only a tiny difference between the  $X_Q$  values in the symmetric rapidity intervals in the projectile and target hemispheres, and slightly stronger effects for

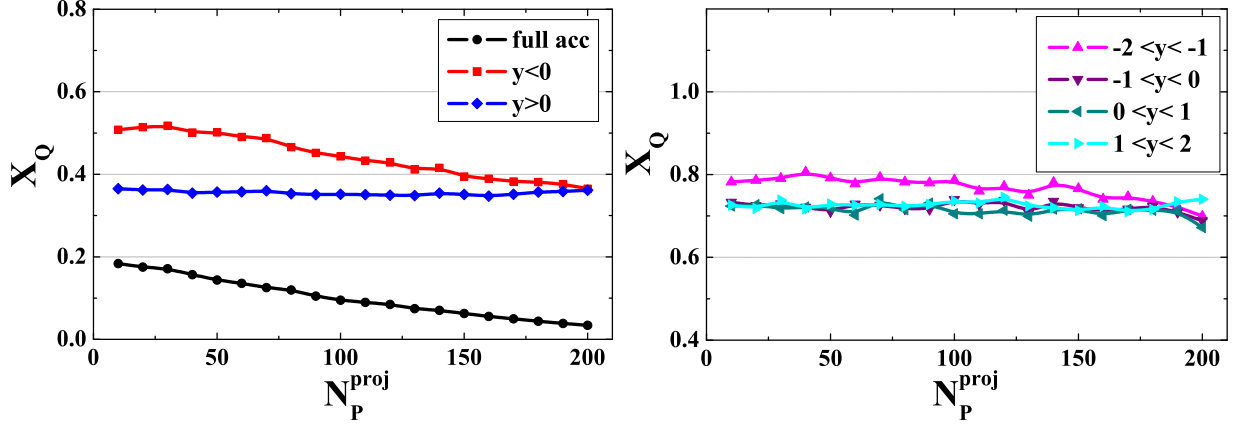


FIG. 9: *Left*: The HSD simulations in Pb+Pb collisions at 158 AGeV for  $X_Q$  at different values of  $N_P^{proj}$  in the full acceptance (lower curve), for the projectile (middle curve) and target (upper curve) hemispheres. *Right*: The same, but for symmetric rapidity intervals in the c.m.s.

the whole projectile and target hemispheres (Fig. 9, right). In fact, the fluctuations of  $N_+$  and  $N_-$  are very different in the projectile and target hemispheres, and the scaled variances  $\omega_+^t$  and  $\omega_-^t$  have a very strong  $N_P^{proj}$ -dependence. This is shown in Fig. 10 obtained in our previous study [17].

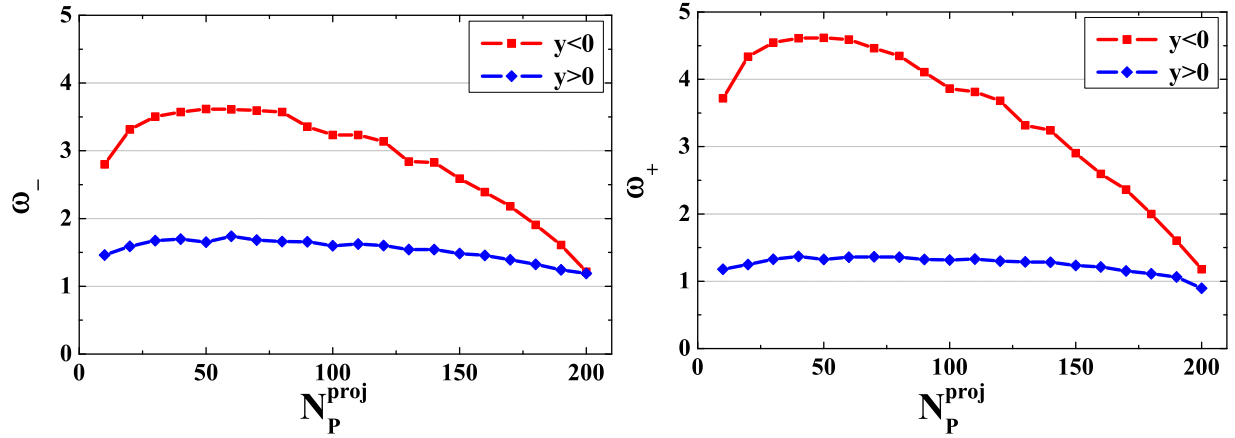


FIG. 10: The HSD results for the scaled variances of negatively (*left*) and positively (*right*) charged hadrons in Pb+Pb collisions at 158 AGeV for the projectile (lower curves) and target (upper curves) hemispheres.

The  $X_Q$  can be presented in two equivalent forms

$$X_Q = \omega_+ \frac{\langle N_+ \rangle}{\langle N_{ch} \rangle} + \omega_- \frac{\langle N_- \rangle}{\langle N_{ch} \rangle} - 2 \frac{\Delta(N_+, N_-)}{\langle N_{ch} \rangle} = 2 \omega_+ \frac{\langle N_+ \rangle}{\langle N_{ch} \rangle} + 2 \omega_- \frac{\langle N_- \rangle}{\langle N_{ch} \rangle} - \omega_{ch} . \quad (12)$$

Eq. (12) is valid for any region of the phase space: full phase space, projectile or target hemisphere, etc. As seen from Fig. 10, both  $\omega_+^t$  and  $\omega_-^t$  are large and strongly  $N_P^{proj}$ -dependent. This is not seen in  $X_Q^t$  because of strong correlations between  $N_+^t$  and  $N_-^t$ , i.e. the term  $2 \Delta(N_+, N_-)/\langle N_{ch} \rangle$  compensates  $\omega_+$  and  $\omega_-$  terms in Eq. (12). This is also seen from Fig. 11. A cancellation of strong  $N_P^{proj}$ -dependence in the target hemisphere takes

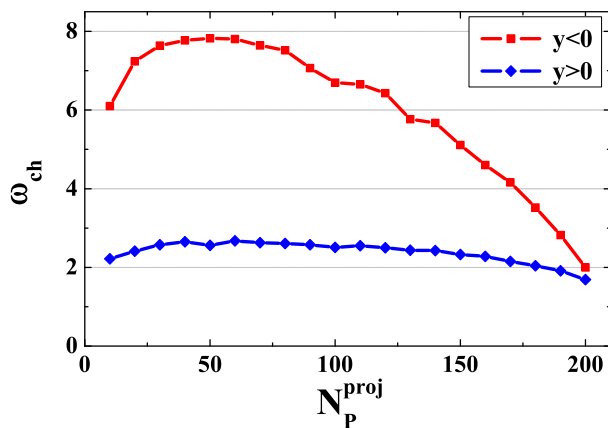


FIG. 11: The HSD results for the scaled variances of all charged hadrons,  $\omega_{ch}$ , in Pb+Pb collisions at 158 AGeV for the projectile (lower curve) and target (upper curve) hemispheres.

place between the sum of  $\omega_+^t$  and  $\omega_-^t$  terms of Eq. (12), and the  $\omega_{ch}^t$ -term.

Fig. 12 shows a comparison of the HSD results for  $X_Q$  with NA49 data in Pb+Pb collisions at 158 AGeV for the forward rapidity interval  $1.1 < y < 2.6$  inside the projectile hemisphere with additional  $p_T$ -filter imposed. As an illustration, the HSD results in the symmetric backward rapidity interval  $-2.6 < y < -1.1$  (target hemisphere) are also included. One observes no difference between the  $X_Q$  results for the NA49 acceptance in the projectile and target hemispheres. The HSD values for  $\omega_+$ ,  $\omega_-$ , and  $\omega_{ch}$  are rather different in the projectile and target hemispheres for the NA49 acceptance (see Figs. 10 and 11). This is not seen in Fig. 12 for  $X_Q$ . As explained above a cancellation between  $\omega_+$ ,  $\omega_-$  and  $\omega_{ch}$  terms take place in Eq. (12). In fact, NA49 did not perform the  $X_Q$  measurements. The  $X_Q$ -data (solid dots) presented in Fig. 12 are obtained from Eq. (12) using the NA49 data for  $\omega_+$ ,  $\omega_-$ , and  $\omega_{ch}$  as

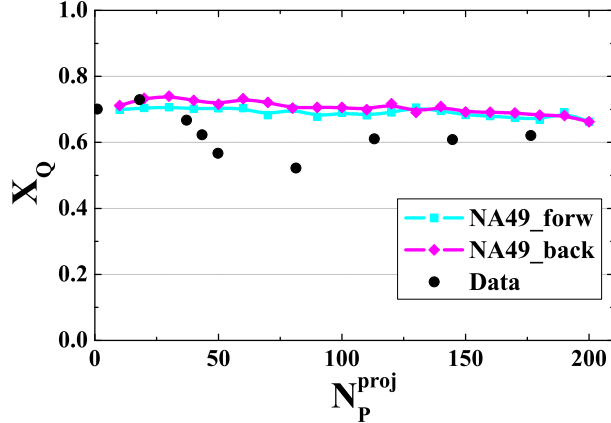


FIG. 12: The HSD results for  $X_Q$  for Pb+Pb collisions at 158 AGeV for the forward rapidity interval  $1.1 < y < 2.6$  inside the projectile hemisphere. The solid dots are the estimates obtained from Eq. 12 using the NA49 experimental data [19] (the errorbars are not indicated here). For illustration, the HSD results in the symmetric backward rapidity interval  $-2.6 < y < -1.1$  (target hemisphere) are also presented.

well as  $\langle N_+ \rangle$ ,  $\langle N_- \rangle$ , and  $\langle N_{ch} \rangle$  [19]. Such a procedure leads, however, to very large errors for  $X_Q$  (which are not indicated in Fig. 12). This makes impossible any conclusion about (dis)agreement of the HSD results with NA49 data.

## V. FLUCTUATIONS IN MOST CENTRAL COLLISIONS

In this section we consider the baryon number and electric charge fluctuations in the symmetric rapidity interval  $[-\Delta y, \Delta y]$  in the c.m.s. for the most central Pb+Pb events. We chose the sample of most central events by restricting the impact parameter to  $b < 2$  fm. It gives about 2% most central Pb+Pb collisions from the whole minimum bias sample. Fig. 13 shows the HSD results for electric charge fluctuations in 2% of most central Pb+Pb collisions for the symmetric rapidity interval  $[-\Delta y, \Delta y]$  in the c.m.s. as the function of  $\Delta y$ . For  $\Delta y \rightarrow 0$  one finds  $X_Q \rightarrow 1$ . This can be understood as follows: For  $\Delta y \rightarrow 0$  the fluctuations of negatively, positively and all charged particles behave as for the Poisson distribution:  $\omega_+ \cong \omega_- \cong \omega_{ch} \cong 1$ . Then from Eq. (12) it follows that  $X_Q \cong 1$ , too. From Fig. 13 (right) one observes that  $\omega_+$ ,  $\omega_-$ , and  $\omega_{ch}$  all increase with increasing interval  $\Delta y$ . However,  $X_Q$  decreases with  $\Delta y$  and because of global  $Q$  conservation it goes approximately

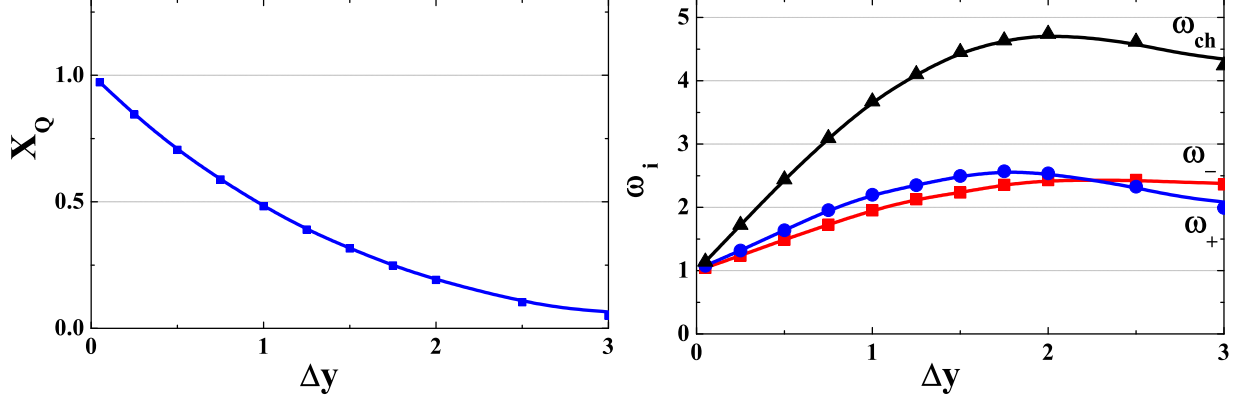


FIG. 13: The HSD results for electric charge fluctuations in 2% most central Pb+Pb collisions at 158 AGeV in the symmetric rapidity interval  $[-\Delta y, \Delta y]$  in the c.m.s. A *left* panel shows the behavior of  $X_Q$ , and a *right* one demonstrates separately  $\omega_+$ ,  $\omega_-$ , and  $\omega_{ch}$ .

to zero when all final particles are accepted.

In Fig. 14 (left) the HSD results for the scaled variances are presented in full acceptance as functions of  $N_P^{proj}$ . Fig.14 (right) demonstrates the probability distribution of events with  $b < 2$  fm over  $N_P^{proj}$ . One observes that even in the 2% centrality sample the values of  $N_P^{proj}$

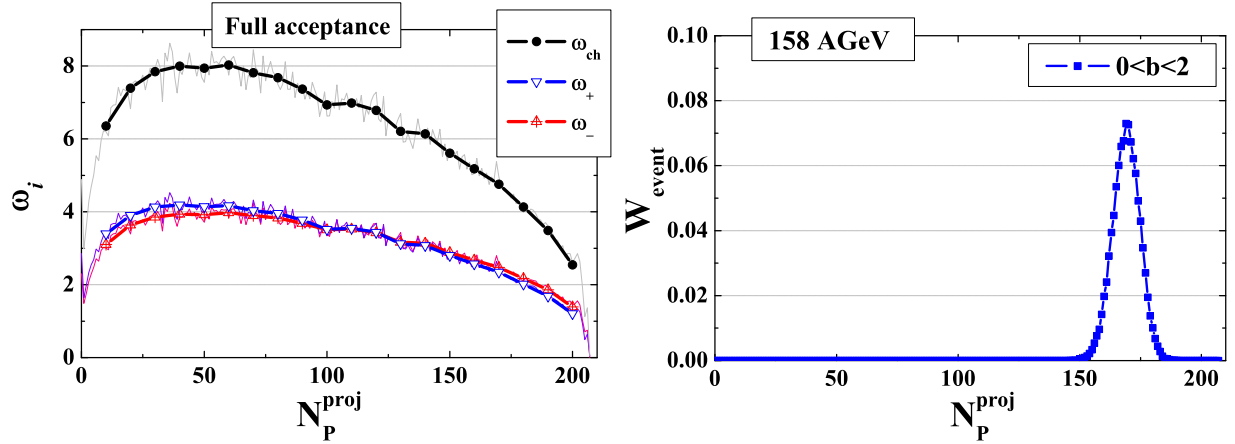


FIG. 14: The HSD results in Pb+Pb collisions at 158 AGeV. *Left*: The scaled variances  $\omega_+$ ,  $\omega_-$ , and  $\omega_{ch}$  in the full acceptance. *Right*: The distributions of events over  $N_P^{proj}$  in most central collisions with  $b < 2$  fm.

are noticeably smaller than the maximum value,  $A = 208$ . As seen from Fig. 14 (left) the HSD values of  $\omega_+$ ,  $\omega_-$ , and  $\omega_{ch}$  become then essentially larger than 1, in agreement with those presented in Fig. 13.

Fig. 15 shows the net baryon number fluctuations in the symmetric rapidity interval  $[-\Delta y, \Delta y]$  in the c.m.s. as the function of  $\Delta y$ . As a measure of the net baryon number

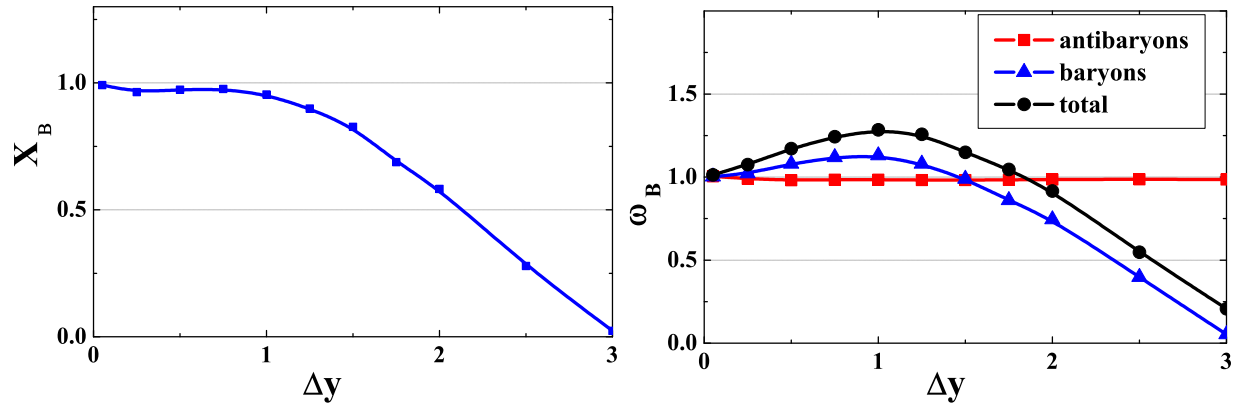


FIG. 15: The HSD results for net baryon number fluctuations in 2% most central Pb+Pb collisions at 158 AGeV in the symmetric rapidity interval  $[-\Delta y, \Delta y]$  in the c.m.s. The *left* panel shows the behavior of  $X_B$ , and a *right* panel presents separately  $\omega_{N_B}$ ,  $\omega_{N_{\bar{B}}}$ , and  $\omega_{N_B + N_{\bar{B}}}$ .

fluctuations we have used the quantity,

$$X_B \equiv \frac{Var(B)}{\langle N_B + N_{\bar{B}} \rangle}. \quad (13)$$

As for electric charge, one finds that  $X_B \rightarrow 1$  at  $\Delta y \rightarrow 0$  (this is because all  $\omega_{N_B}$ ,  $\omega_{N_{\bar{B}}}$ , and  $\omega_{N_B + N_{\bar{B}}}$  go to 1 in this limit (see Fig. 15, left), and  $X_B \rightarrow 0$  at upper limit of  $\Delta y$  because of global baryon number conservation.

Writing the variance  $Var(B)$  in the form,

$$Var(B) = 2 Var(N_B) + 2 Var(N_{\bar{B}}) - Var(N_B + N_{\bar{B}}), \quad (14)$$

we find

$$X_B = 2 \omega_{N_B} \frac{\langle N_B \rangle}{\langle N_B + N_{\bar{B}} \rangle} + 2 \omega_{N_{\bar{B}}} \frac{\langle N_{\bar{B}} \rangle}{\langle N_B + N_{\bar{B}} \rangle} - \omega_{N_B + N_{\bar{B}}}. \quad (15)$$

The behavior of the different terms in Eq. (15) is the following: As seen from Fig. 15, right,  $\omega_{N_{\bar{B}}} \cong 1$  for all values of  $\Delta y$ . This is because  $N_{\bar{B}} \ll N_B$ , and baryon number conservation does not affect the fluctuations of antibaryons. Due to the small number of antibaryons in comparison to baryons, one also observes  $\omega_B \cong \omega_{N_B} \cong \omega_{N_B + N_{\bar{B}}}$ .

## VI. SUMMARY AND CONCLUSIONS

The event-by-event fluctuations in Pb+Pb collisions at 158 AGeV have been studied within the HSD transport model. Studies of baryon number, electric charge and hadron multiplicity fluctuations give a unique possibility to investigate the early stage dynamics of initial flows in the colliding nuclei.

It has been found that the fluctuations of the number of target participants strongly influence the baryon number and charged multiplicity fluctuations. The consequences of this fact depend crucially on the dynamics of the initial flows of the conserved charges and inelastic energy.

The existing models of nucleus-nucleus collisions can be divided into 3 limiting groups: transparency, mixing and reflection. The HSD transport model is close to transparency models for both the flows of baryon number and hadron production sources.

New information comes from the data for  $\omega_i$  in A+A collisions. The data are urgently needed for different  $i$ -particles, different  $A$ , different acceptances (both in the target and projectile hemispheres), different centralities (and different centrality triggers), and at different collision energies.

### Acknowledgments

We like to thank W. Cassing, M. Gaździcki, B. Lungwitz, I.N. Mishustin, St. Mrówczyński, M. Rybczyński, and L.M. Satarov for numerous discussions. The work was supported in part by US Civilian Research and Development Foundation (CRDF) Cooperative Grants Program, Project Agreement UKP1-2613-KV-04.

- 
- [1] W. Ehehalt and W. Cassing, Nucl. Phys. A **602**, 449 (1996); W. Cassing and E.L. Bratkovskaya, Phys. Rep. **308**, 65 (1999); W. Cassing, E. L. Bratkovskaya, and A. Sibirtsev, Nucl. Phys. A **691**, 753 (2001).
  - [2] H. Weber, E. L. Bratkovskaya, W. Cassing, and H. Stöcker, Phys. Rev. **C67**, 014904 (2003); E. L. Bratkovskaya, M. Bleicher, M. Reiter, S. Soff, H. Stöcker, M. van Leeuwen, S. A. Bass, and W. Cassing, Phys. Rev. **C69**, 054907 (2004); E. L. Bratkovskaya, M. Bleicher, W. Cassing,

- M. Reiter, S. Soff, H. Stöcker, Prog. Part. Nucl. Phys. **53**, 225 (2004); E. L. Bratkovskaya, W. Cassing, and H. Stöcker, Phys. Rev. C **67**, 054905 (2003).
- [3] M. Gaździcki and St. Mrówczyński, Z. Phys. C **26**, 127 (1992);
- [4] L. Stodolsky, Phys. Rev. Lett. **75**, 1044 (1995); E.V. Shuryak, Phys. Lett. B **423**, 9 (1998); St. Mrówczyński, Phys. Lett. B **430**, 9 (1998).
- [5] G. Baym and H. Heiselberg, Phys. Lett. B **469**, 7 (1999).
- [6] I.N. Mishustin, Phys. Rev. Lett. **82**, 4779 (1999); Nucl. Phys. A **681**, 56c (2001); H. Heiselberg and A.D. Jackson, Phys. Rev. C **63**, 064904 (2001).
- [7] M.A. Stephanov, K. Rajagopal, and E.V. Shuryak, Phys. Rev. Lett. **81**, 4816 (1998); Phys. Rev. D **60**, 114028 (1999); M.A. Stephanov, Acta Phys. Polon. B **35**, 2939 (2004).
- [8] S. Jeon and V. Koch, Phys. Rev. Lett. **83**, 5435 (1999); *ibid.* **85**, 2076 (2000).
- [9] H. Heiselberg, Phys. Rep. **351**, 161 (2001).
- [10] S. Jeon and V. Koch, hep-ph/0304012, Review for Quark-Gluon Plasma 3, eds. R.C. Hwa and X.-N. Wang, World Scientific, Singapore.
- [11] M. Bleicher *et al.*, Nucl. Phys. A **638**, 391 (1998); Phys. Lett. B **435**, 9 (1998); Phys. Rev. C **62**, 061902 (2000); *ibid.* **62**, 041901 (2000); S. Jeon, L. Shi, and M. Bleicher, nucl-th/0506025; S. Haussler, H. Stoecker, and M. Bleicher, hep-ph/0507189.
- [12] M. Gaździcki, M.I. Gorenstein, and St. Mrówczyński, Phys. Lett. B **585**, 115 (2004); M.I. Gorenstein, M. Gaździcki, and O.S. Zozulya, *ibid.* **585**, 237 (2004); M. Gaździcki, nucl-ex/0507017.
- [13] H. Stöcker and W. Greiner, Phys. Rep. **137**, 277 (1986); J. Cleymans and H. Satz, Z. Phys. C **57**, 135 (1993); J. Sollfrank, M. Gaździcki, U. Heinz, and J. Rafelski, *ibid.* **61**, 659 (1994); G.D. Yen, M.I. Gorenstein, W. Greiner, and S.N. Yang, Phys. Rev. C **56**, 2210 (1997); F. Becattini, M. Gaździcki, and J. Sollfrank, Eur. Phys. J. C **5**, 143 (1998); G.D. Yen and M.I. Gorenstein, Phys. Rev. C **59**, 2788 (1999); P. Braun-Munzinger, I. Heppe and J. Stachel, Phys. Lett. B **465**, 15 (1999); P. Braun-Munzinger, D. Magestro, K. Redlich, and J. Stachel, *ibid.* **518**, 41(2001); F. Becattini, M. Gaździcki, A. Keränen, J. Manninen, and R. Stock, Phys. Rev. C **69**, 024905 (2004).
- [14] P. Braun-Munzinger, K. Redlich, J. Stachel, nucl-th/0304013, Review for Quark Gluon Plasma 3, eds. R.C. Hwa and X.-N. Wang, World Scientific, Singapore.
- [15] F. Becattini, Z. Phys. C **69**, 485 (1996); F. Becattini, U. Heinz, *ibid.* **76**, 269 (1997); F.

- Becattini, G. Passaleva, Eur. Phys. J. C **23**, 551 (2002).
- [16] V.V. Begun, M. Gaździcki, M.I. Gorenstein, and O.S. Zozulya, Phys. Rev. C **70**, 034901 (2004); V.V. Begun, M.I. Gorenstein, and O.S. Zozulya, Phys. Rev. C **72**, 014902 (2005); A. Keränen, F. Becattini, V.V. Begun, M.I. Gorenstein, and O.S. Zozulya, J. Phys. G **31**, S1095 (2005); F. Becattini, A. Keränen, L. Ferroni, T. Gabbriellini, Phys. Rev. C **72**, 064904 (2005); V.V. Begun, M.I. Gorenstein, A.P. Kostyuk, and O.S. Zozulya, Phys. Rev. C **71**, 054904 (2005); J. Cleymans, K. Redlich, L. Turko, Phys. Rev. C **71**, 047902 (2005); J. Cleymans, K. Redlich, L. Turko, J. Phys. G **31**, 1421-1435 (2005); V.V. Begun, M.I. Gorenstein, A.P. Kostyuk, and O.S. Zozulya, J. Phys. G **32**, 935 (2006). V.V. Begun and M.I. Gorenstein, Phys. Rev. C **73** 054904 (2006).
- [17] V.P. Konchakovski, S. Haussler, M.I. Gorenstein, E.L. Bratkovskaya, M. Bleicher, and H. Stöcker, Phys. Rev. C **73**, 034902 (2006).
- [18] M. Gaździcki and M.I. Gorenstein, hep-ph/0511058.
- [19] M. Rybczynski *et al.* [NA49 Collaboration], J. Phys. Conf. Ser. **5**, 74 (2005); T. Anticic *et al.* [NA49 Collaboration], Phys. Rev. C **70**, 034902 (2004); P. Dinkelaker [NA49 Collaboration], J. Phys. G **31**, S1131 (2005).